



## Electrolytic production of Cu–Ni alloys in $\text{CaCl}_2\text{–Cu}_2\text{S–NiS}$ molten salt

Levent KARTAL<sup>1,2</sup>, Servet TIMUR<sup>1</sup>

1. Department of Metallurgical & Materials Engineering, Istanbul Technical University, 34469 Maslak, Istanbul, Turkey;
2. Department of Metallurgical & Materials Engineering, Corum, Hitit University, Turkey

Received 15 November 2017; accepted 14 August 2018

**Abstract:** An alternative metal/alloy production method, known as direct electrochemical reduction (DER), was introduced for the fabrication of CuNi alloys from mixed sulfides ( $\text{Cu}_2\text{S}$ , NiS) under both galvanostatic and potentiostatic conditions. The influences of the process parameters (e.g., cell voltage and current) on the compositions of the reduced compounds were investigated to yield industrially desirable alloys, namely, CuNi10, CuNi20, and CuNi30. The electrochemical behaviors of  $\text{Cu}_2\text{S}$  and NiS in  $\text{CaCl}_2$  melt were examined at a temperature of 1200 °C via cyclic voltammetry (CV). Based on the CV results, the cathodic reduction of  $\text{Cu}_2\text{S}$  occurred in one step and cathodic reductions of NiS occurred in two steps, i.e.,  $\text{Cu}_2\text{S} \Rightarrow \text{Cu}$  for copper reduction and  $\text{NiS} \Rightarrow \text{Ni}_3\text{S}_2 \Rightarrow \text{Ni}$  for nickel reduction. Galvanostatic studies revealed that it was possible to fabricate high-purity CuNi10 alloys containing a maximum sulfur content of  $320 \times 10^{-6}$  via electrolysis at 10 A for 15 min. Scanning electron microscopy along with energy-dispersive X-ray spectrometry and optical emission spectroscopy (OES) examinations showed that it was possible to fabricate CuNi alloys of preferred compositions and with low levels of impurities, i.e., less than  $60 \times 10^{-6}$  sulfur, via DER at 2.5 V for 15 min.

**Key words:** molten salt electrolysis; electro-reduction; copper extraction; copper sulfide; nickel sulfide; Cu–Ni alloys

### 1 Introduction

Copper–nickel (Cu–Ni) alloys have been commonly used in many different industries, namely, shipping, offshore oil, gas production, and desalination and for the fabrication of silver-colored coins, electrical resistors, and heater elements due to their outstanding properties such as high corrosion resistance against seawater, tarnish resistance, color, and resistivity [1–3].

Copper and nickel are industrially produced according to multi-step pyrometallurgical processes in which sulfide ores are processed via smelting and conversion operations. In these procedures, Cu–Ni–Fe–S concentrates are turned into mattes with high Cu, Ni, and Cu–Ni contents. The conversion of mattes into their metal forms is performed in two steps for nickel and copper at ~1600 and ~1200 °C, respectively. Such high-energy and high-temperature methods require considerable capital investment, time, and labor as well as extra precautions to avoid potential environmental issues, such as  $\text{SO}_2$  emission [4–6]. Formation of  $\text{SO}_2$  as a by-product is always considered as a significant

problem even though it is possible to be captured in the form of sulfuric acid using modern, expensive  $\text{SO}_2$  capture systems [6,7]. As an alternative to conventional extraction methods, a new metal production approach for titanium was introduced in the late 1990s, in which electro-reduction reactions occur on cathodically polarized titanium dioxide pellets to produce metallic titanium. This direct electrochemical reduction (DER) process has attracted considerable attention due to its fewer number of processing stages, less labor requirement, and low energy consumption as well as its simplicity and feasibility for small-scale applications [8–13]. Therefore, many attempts have been made to adopt this method for the production of other metals (Fe, Nb, Cr, etc.) [14–16] and alloys (Fe–Ti, ZrMn<sub>2</sub>, CeCo<sub>5</sub>, Mg–Sr, Mg–Li–La, TiNbTaZr, etc.) [17–22]. During DER, the reduced metal remains as a solid phase on the cathode holder, whereas  $\text{O}^{2-}$  on the cathodically polarized charged material transfers to the anode(s) to oxidize as  $\text{CO}/\text{CO}_2$  in the case of graphite anode(s) [23–28].

According to a principle similar to the DER of oxides, it is possible to reduce metal sulfides to their

metallic forms, where  $S^{2-}$  transfers to the anode(s) to discharge as elemental sulfur gas. To date, very few electrolytic reduction studies have been conducted for metal sulfides [29]. For instance, the productions of molybdenum [30,31], aluminum [32], tungsten [33], antimony [34], titanium [35], vanadium [36], copper–iron [37], and copper [29,38,39] from their sulfides were investigated.

In this study, for the first time, we examine the electrolytic production of copper–nickel alloys from their sulfides ( $Cu_2S$  and  $NiS$ ) in  $CaCl_2$  electrolyte. Accordingly, the possibility of controlled CuNi alloy production with different compositions and the reduction mechanism of  $Cu_2S$ – $NiS$  mixtures have been explored using cyclic voltammetry (CV) and galvanostatic and potentiostatic methods. The technique suggested in this study can also be used for the recovery of heavy metals from their precipitated sulfides, which are frequently produced in the mining and metallurgical industries during the treatment of process solutions, waste waters, and mining effluents [40].

## 2 Experimental

The materials used in this study are listed in Table 1 with their specifications. The schematic depiction of the experimental setup utilized for the molten salt electrolysis is shown in Fig. 1.

**Table 1** Materials used in cyclic voltammetry measurements and molten salt electrolysis

Material	Form	Specification
$Cu_2S$	Powder	30 $\mu m$ (average particle size)
$NiS$	Powder	30 $\mu m$ (average particle size)
$CaCl_2$	Powder	Dried at 150 °C
Reference electrode	Graphite rod	$d6$ mm, with 99.9% purity
Working electrode (WE)	Tungsten wire	$d1$ mm, with 99.9% purity
Counter electrode (CE)	Graphite rod	$d6$ mm, with 99.9% purity
Cathode	Graphite crucible	Outer diameter 60 mm, internal diameter 45 mm, height 100 mm
Anode	Graphite rod	$d16$ mm, with 99.9% purity

During electrolysis, a graphite rod was used as the anode and a graphite crucible containing a mixture of  $Cu_2S$ ,  $NiS$ , and  $CaCl_2$  was polarized as the cathode.

$CaCl_2$ , utilized as the electrolyte, was kept in an oven at 150 °C to prevent re-moistening.  $CaCl_2$  granules were filled into the graphite crucible, which was then heated in a medium-frequency induction furnace (50 kHz, 30 kW, 40 A). Before starting heating, the electrolysis cell was purged with highly pure argon (99.9% purity) at a flow rate of 50 mL/min. Then, the temperature of the system was increased to 1200 °C and maintained for 30 min to ensure the homogenization of the electrolyte before initiating electrolysis.

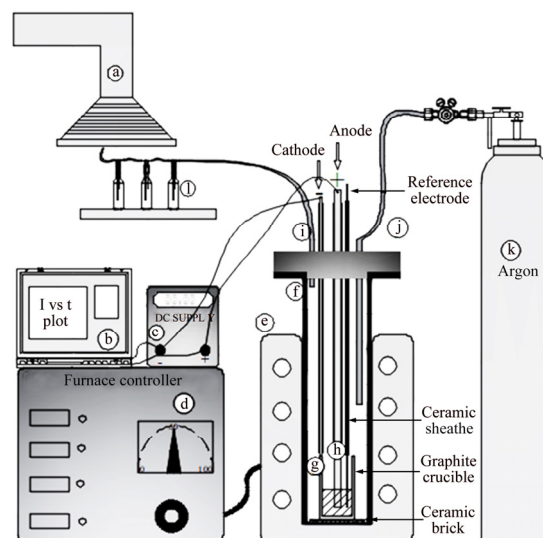


**Fig. 1** Schematic illustration of experimental setup: (a) Fume hood; (b) Data acquisition system; (c) DC supply; (d) Furnace controller; (e) Induction furnace; (f) Alumina vessel; (g) Graphite crucible cathode; (h) Graphite rod anode; (i) Gas outlet; (j) Gas inlet; (k) Argon cylinder; (l) Gas washing bottle

The mechanism of the DER of  $Cu_2S$ – $NiS$  was further investigated via CV. The  $CaCl_2$ – $Cu_2S$ – $NiS$  melt was left for 30 min to achieve equilibration of the constituents before performing CV analysis. The CV measurements were conducted on a Gamry reference 3000 electrochemical workstation. A tungsten wire was used as the WE, and graphite rods were used as the CE and the quasi-reference electrode. The cyclic voltammograms of the system were obtained at 1200 °C with a scanning rate of 200 mV/s.

In addition to the CV measurement, electrolysis at constant current and voltage was performed according to the experimental conditions listed in Table 2. After the electrolysis, the extracted cathode products accumulated at the bottom of the graphite crucible were poured into a graphite mold. The mold was cooled down to room temperature, and the solidified electrolyte on the cathode product was crushed and washed with hot water.

The obtained products were analyzed using optical emission spectroscopy (OES, GNR-S7 MLP), X-ray diffraction (XRD, Siemens D5000), and scanning

electron microscopy (SEM, JSM-840, JEOL) equipped with energy-dispersive X-ray spectrometry (EDS, EDS link, Oxford).

**Table 2** Experimental conditions for molten salt electrolysis conducted at 1200 °C

Cu/Ni mass ratio	Current/A	Cell voltage/V	Time/min
9:1	5	–	30
9:1	10	–	15
9:1	–	1	30
9:1	–	1.5	15
8:2	–	1.5	15
7:3	–	1.5	15
9:1	–	2.0	15
9:1	–	2.5	15

### 3 Result and discussion

#### 3.1 Cyclic voltammetry

Table 3 gives the Gibbs free energy change in the copper and nickel sulfides as well as in calcium chloride at 1200 °C calculated using HSC chemistry 5.1 version. The decomposition potentials were additionally derived from the given standard Gibbs free energy at 1200 °C. Since the decomposition potentials of the Cu and Ni sulfides were much lower than that of CaCl<sub>2</sub>, the reduction of Cu and Ni was expected to occur without any Cl<sub>2</sub> emission.

**Table 3** Gibbs free energy change ( $\Delta G^\ominus$ ) along with decomposition voltages of Cu and Ni sulfides and CaCl<sub>2</sub> at 1200 °C

Reaction	$\Delta G^\ominus/(\text{kJ}\cdot\text{mol}^{-1})$	Theoretical decomposition voltage/V
$\text{CaCl}_2=\text{Ca}+\text{Cl}_2(\text{g})$	588.414	-3.05
$\text{Cu}_2\text{S}=2\text{Cu}+1/2\text{S}_2(\text{g})$	89.441	-0.46
$\text{NiS}=\text{Ni}+1/2\text{S}_2(\text{g})$	38.761	-0.20
$3\text{NiS}=\text{Ni}_3\text{S}_2+1/2\text{S}_2(\text{g})$	-27.251	0.14
$\text{Ni}_3\text{S}_2=3\text{Ni}+\text{S}_2(\text{g})$	143.533	-0.24

The electrochemical behaviors of Cu<sub>2</sub>S and NiS in molten CaCl<sub>2</sub> were studied using CV. The cyclic voltammograms of the system obtained at 1200 °C and a scanning rate of 200 mV/s are shown in Figs. 2 and 3. As shown by the theoretical decomposition voltage values (Table 3) and CV diagrams (Figs. 2 and 3), the reduction voltages of the Cu and Ni sulfides significantly changed. Noteworthy differences between these theoretical and practical values could be attributed to the kinetics and dynamics of the cathode reactions. Generally, cell

reactions for molten salt electrolysis containing MeS are given as follows [29,33]:

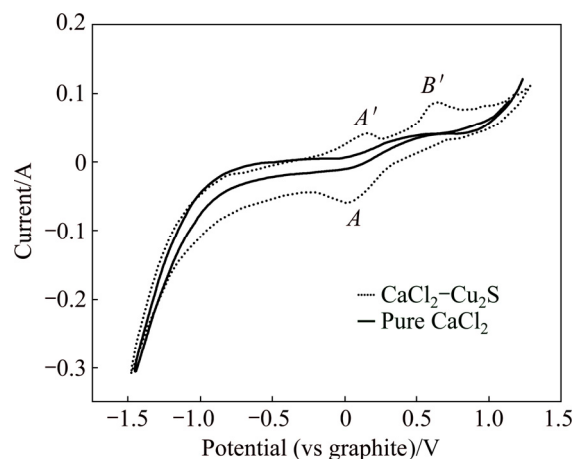
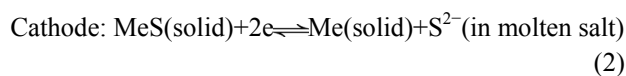


**Fig. 2** Cyclic voltammogram in pure CaCl<sub>2</sub> and CaCl<sub>2</sub>-Cu<sub>2</sub>S mixture at 1200 °C (WE:  $A=0.32 \text{ cm}^2$ ; CE: scan rate=200 mV/s)

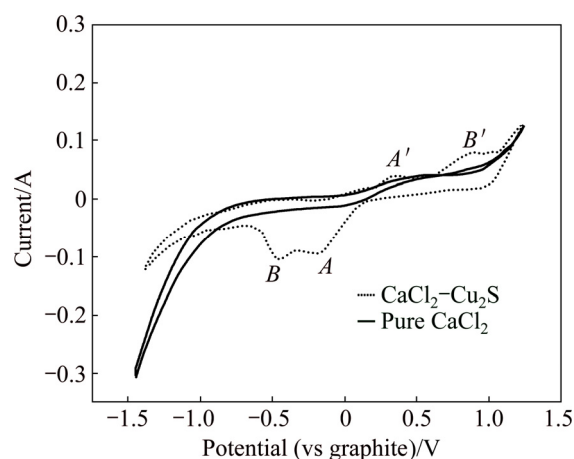
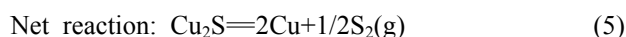
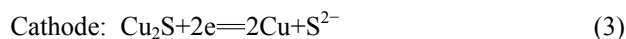


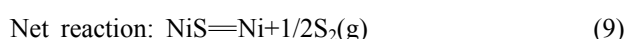
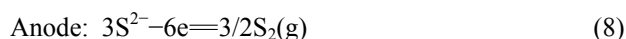
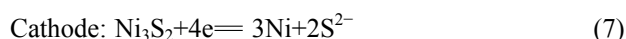
**Fig. 3** Cyclic voltammogram in pure CaCl<sub>2</sub> and CaCl<sub>2</sub>-NiS mixture at 1200 °C (WE:  $A=0.32 \text{ cm}^2$ ; CE: scan rate=200 mV/s)

The CV results of Cu<sub>2</sub>S showed a wide reduction peak at 0.05 V, labeled as A. On the anodic side of the CV, the minimum oxidation current was approximately -0.20 V and it peaked at 0.15 V, marked as A'. After A', another oxidation process was observed at about 0.67 V, labeled as B'. It was apparent that the electrodesulfidation of Cu<sub>2</sub>S proceeded in at one-step, as described below:



In the absence of NiS, no obvious redox peaks were observed in the potential range of -1.5 V to 1.0 V.

However, after adding 3 g NiS into the CaCl<sub>2</sub> melt, two reduction peaks at about -0.20 V (peak *A*) and -0.45 V (peak *B*) appeared during the negative scan (blue line in Fig. 3). The reason for the appearance of these two sequential peaks could be the stepwise reduction of NiS. First, NiS was partially dissociated to Ni<sub>3</sub>S<sub>2</sub> and S<sup>2-</sup> in molten chlorides, and newly formed Ni<sub>3</sub>S<sub>2</sub> was then reduced to Ni:



Lastly, the voltammetric behavior of mixed Cu<sub>2</sub>S/NiS in molten CaCl<sub>2</sub> at 1200 °C was investigated to understand the electro-reduction mechanism of mixed sulfides (Fig. 4). The reduction of the mixed CaCl<sub>2</sub>-Cu<sub>2</sub>S-NiS melt initiated at about 0.10 V, as seen in the CaCl<sub>2</sub>-NiS mixture (Fig. 3). Peak *A* was possibly caused by the formation of Cu-Ni<sub>3</sub>S<sub>2</sub> compounds from the reduction of Cu<sub>2</sub>S and NiS. After peak *A*, another reduction process started at about -0.30 V (marked as *B*), which was probably due to the formation of Ni reduced from Ni<sub>3</sub>S<sub>2</sub>. During the positive scan, oxidation peaks *A'*, *B'*, and *C'* at about 0.35, 0.5, and 0.90 V were observed, which were likely belonged to the oxidation of Cu, Cu<sub>2</sub>S-Ni and Ni<sub>3</sub>S<sub>2</sub>, respectively.

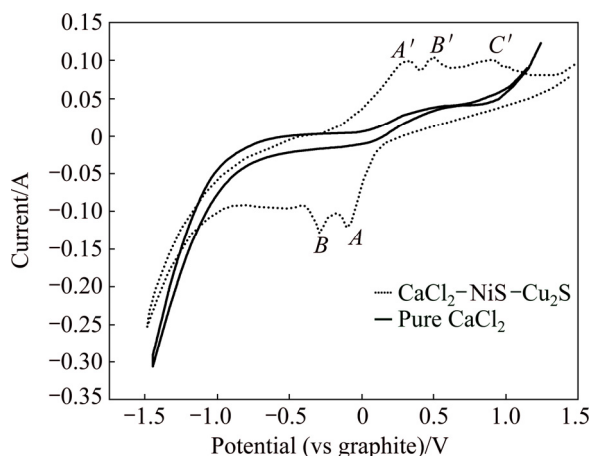


**Fig. 4** Cyclic voltammogram in pure CaCl<sub>2</sub> and CaCl<sub>2</sub>-Cu<sub>2</sub>S-NiS mixture at 1200 °C (WE: *A*=0.32 cm<sup>2</sup>, CE: scan rate= 200 mV/s)

### 3.2 Galvanostatic electrolysis

The electrochemical production of Cu-Ni alloys via the DER technique was initially performed at constant currents of 10 and 5 A.

The cell potential variation as a function of electrolysis time exhibited a sharp increase after considerable reduction of the charged Cu<sub>2</sub>S/NiS powders (Fig. 5). As expected, the cell potential was low

at relatively low currents. A sharp jump was observed after 20 min of electrolysis at 5 A, whereas relatively less increment was observed for electrolysis at 10 A beyond about 10 min.

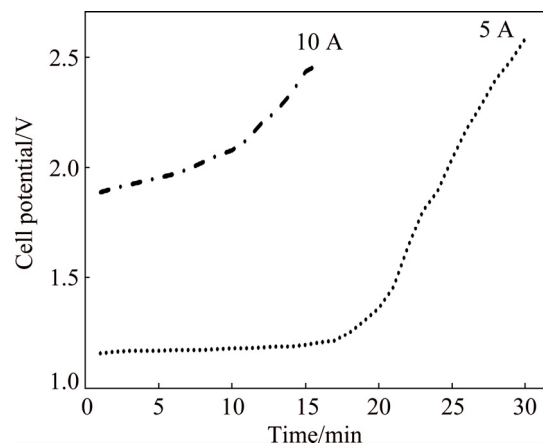


**Fig. 5** Cell voltage versus time in CaCl<sub>2</sub>-Cu<sub>2</sub>S-NiS melt at 1200 °C

The OES results of the produced alloys and the starting mixture ratios are given in Table 4. Apparently, the amount of applied current did not significantly influence the chemistry of the Cu-Ni alloys. As shown in the OES results, the overall matrix compositions obtained at 5 A were close to 9:1 for Cu/Ni (Table 4). Hence, the macro investigation confirmed the composition of the alloys. The chemical composition of the obtained Cu-Ni alloy was close to the Cu/Ni mass ratio in the charged sulfide powder mixture.

**Table 4** Molten salt electrolysis under galvanostatic conditions and product compositions obtained in CaCl<sub>2</sub>-Cu<sub>2</sub>S-NiS melt at 1200 °C

No.	Cu/Ni mass ratio	Current/A	Time/min	Mass fraction/%			
				Cu	Ni	Fe	S
1	9:1	5	30	87.046	11.942	0.567	0.029
2	9:1	10	15	88.077	11.215	0.488	0.032

The microstructures of the products are given in Fig. 6 along with the EDS results. The background light-gray phase (denoted by *B*) was composed of 85.71% Cu and 13.86% Ni, whereas the dark gray regions (denoted by *A*) were composed of 34.92% Cu, 62.09% Ni, and 2.8% Fe. It was shown that a small amount of iron was also collected at the cathode. Interestingly, there were no dark gray areas detected in the sample synthesized at 10 A. The general chemical composition was calculated to be 86.59% Cu, 12.88% Ni, and 0.53% Fe. The possible reason for this diverse microstructure was the high reduction rate at a higher current.

### 3.3 Potentiostatic electrolysis

The cell potentials increased significantly with time in the constant current experiments. In these cases, the potentials could reach the decomposition potentials of the melt. To avoid the decomposition of  $\text{CaCl}_2$ , a second series of experiments were performed at constant voltages. Based on the theoretical calculations (see Table 3,  $\sim 3.05$  V for  $\text{CaCl}_2$  at  $1200^\circ\text{C}$ ) and the CV results, cell voltages of 1.0, 1.5, 2.0, and 2.5 V were chosen. Figure 7 shows the current variations as a function of electrolysis time at different voltages. Apparently, all current curves recorded at different voltages exhibited similar characteristics in that initial high current decreased with time and reached stable values eventually. The electrolysis reached the steady-state background current level after 10 min for all applied voltages.

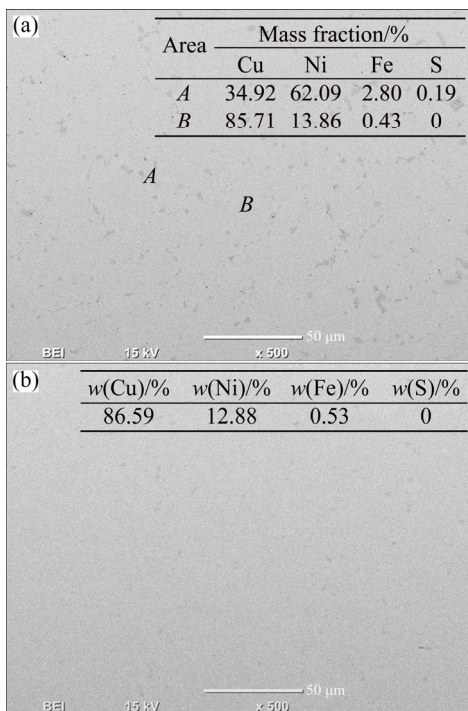


**Fig. 6** SEM images of samples synthesized at 5 A (a) and 10 A (b) in  $\text{CaCl}_2\text{-Cu}_2\text{S-NiS}$  melt at  $1200^\circ\text{C}$

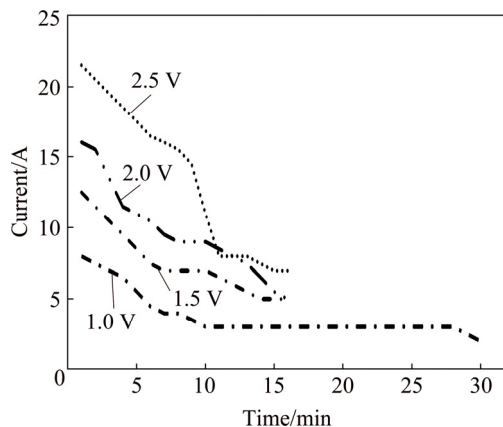


**Fig. 7** Current versus time at different voltages in  $\text{CaCl}_2\text{-Cu}_2\text{S-NiS}$  melt at  $1200^\circ\text{C}$  for Cu/Ni mass ratio of 9:1

The chemical analysis of the obtained products revealed that the Cu, Ni and Fe contents were 88%, 11%–12%, and 0.35%, respectively (Table 5). The sulfur content of the alloys decreased to less than 0.3%.

**Table 5** Chemical analysis of obtained products via OES

Cell voltage/V	Time/min	Mass fraction/%			
		Cu	Ni	Fe	S
1.0	30	88.007	11.282	0.3744	0.255
1.5	15	88.095	11.006	0.3545	0.215
2.0	15	88.235	11.285	0.3463	0.050
2.5	15	87.352	12.188	0.3761	0.006

SEM with EDS analysis (Fig. 8(a)) showed the uniform structure of the synthesized copper–nickel alloys (denoted by *B*) with small Ni–Cu–Fe–S-rich islands (denoted by *A*). An optical image of the same sample revealed that the enrichment of the Ni–Fe–S phases occurred at the grain boundaries (Fig. 8(b)). Minor iron contamination of less than 0.5% was detected in the synthesized products due to the iron content in the initial raw material and the wide range of working voltages, which covered the iron reduction potential. Based on the metallographic analysis and EDS results, it could be deduced that the  $\text{Cu}_2\text{S-NiS}$  mixture in the  $\text{CaCl}_2$  melt could be converted into high-purity CuNi alloys (99%) in a short period of time (i.e., 15 min).

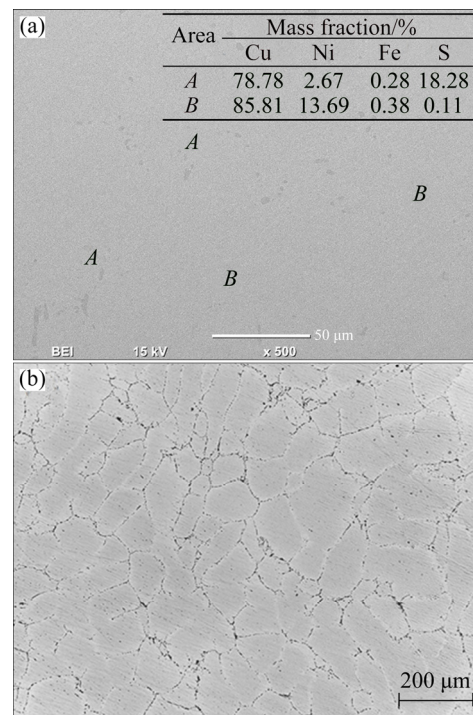


**Fig. 8** SEM image of reduced sample at cell potential of 1.5 V along with EDS analyses (a) and optical micrograph after electrolysis in  $\text{CaCl}_2\text{-Cu}_2\text{S-NiS}$  melt at  $1200^\circ\text{C}$  for 15 min (b)

The entrapped Ni–Cu–S phases could be fully separated from the converted metallic parts by a slow cooling method after pouring the molten mixture into the graphite mold. This problem could be easily overcome for further industrial implementation by integrating a controlled cooling system. With this attachment, the light density of the Ni–Cu–S matte phase accumulated on the top surface of the solidified alloys.

### 3.4 Influence of Cu/Ni ratio on Cu–Ni alloy production

The influence of the Cu/Ni ratio on the composition of the Cu–Ni alloys was studied at constant voltage (1.5 V). As observed in the current variations with respect to electrolysis time given in Fig. 9, the initial current values exhibited declining trends, which was probably due to the same reason as that in the galvanostatic experiments, namely, the almost complete reduction of charged sulfide mixtures. There were three main areas in the current–time curve: sharp decline region I, stable constant current region II, and decreasing trend III. These current tendencies with time indicated the reduction rates of the charged particles. The reductions initiated with relatively high rates (I) and reached steady conditions (II) and were finally completed with decreasing rates (III). The reduction of CuNi10, CuNi20, and CuNi30 showed behaviors similar to that observed in their current–time curves: the higher the nickel content, the larger the region II was.

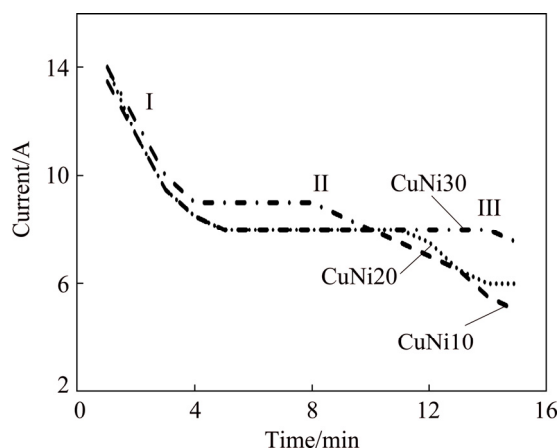


**Fig. 9** Current versus electrolysis time at different Cu/Ni ratios in  $\text{CaCl}_2\text{-Cu}_2\text{S-NiS}$  melt at 1200 °C and 1.5 V for 15 min

According to the OES results (Table 6), the charged  $\text{Cu}_2\text{S/NiS}$  powder mixtures were mostly converted into their metallic forms. SEM with EDS analyses of the products revealed (Fig. 10) that the darker small areas were mainly composed of unreduced  $\text{Cu}_2\text{S-NiS}$  powder (denoted by *A*) and the lighter regions (labeled as *B*) had compositions similar to the relevant Cu–Ni alloys. It should be noted that very small amounts of S remained

in the dark areas. Based on the SEM-EDS and OES results, it could be concluded that the white background in the three produced alloys had a composition similar to the CuNi10, CuNi20, and CuNi30 alloys with heterogeneously distributed unreduced  $\text{Cu}_2\text{S-NiS}$  areas.

Figure 11 showed that higher nickel content in the synthesized alloys resulted in Cu peak shifts to the right side with (220) orientational growth.

**Table 6** OES results of CuNi10, CuNi20, and CuNi30 alloys synthesized in  $\text{CaCl}_2$  melt at 1200 °C and 1.5 V for 15 min

Cu/Ni mass ratio	Mass fraction/%			
	Cu	Ni	Fe	S
9:1	88.095	11.006	0.3545	<0.3
8:2	77.007	22.005	0.3915	<0.3
7:3	67.095	31.186	0.3610	1.150

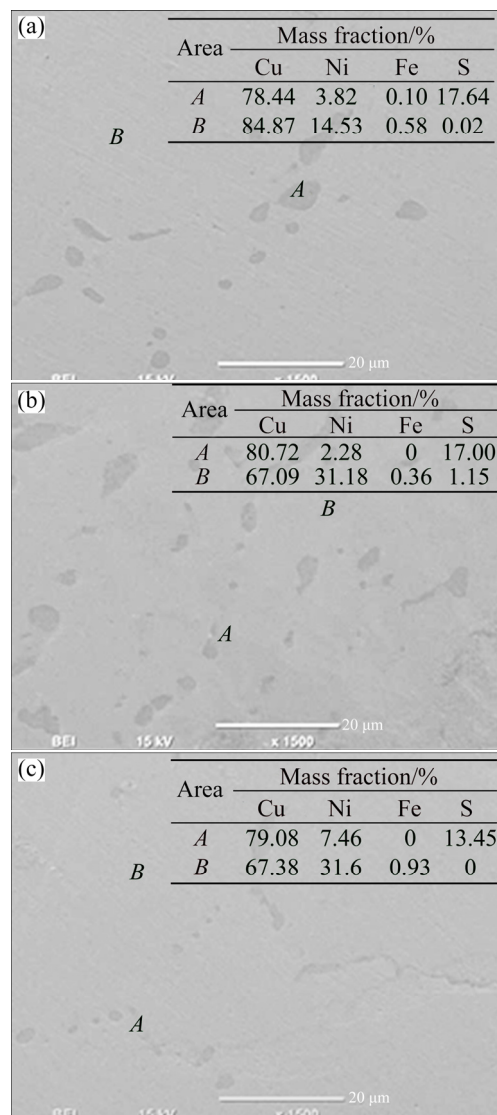


**Fig. 10** SEM images of alloys produced at different Cu/Ni mass ratios in  $\text{CaCl}_2\text{-Cu}_2\text{S-NiS}$  melt at 1200 °C and 1.5 V for 15 min: (a) 9:1; (b) 8:2; (c) 7:3

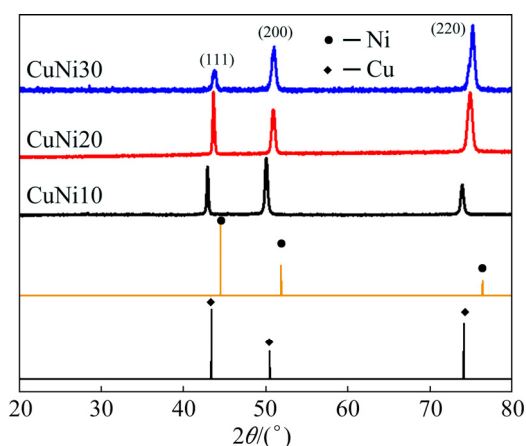


**Fig. 11** XRD patterns of Cu–Ni alloys synthesized at different Cu/Ni ratios in  $\text{CaCl}_2\text{--Cu}_2\text{S--NiS}$  melt at 1200 °C and 1.5 V for 15 min

## 4 Conclusions

1) According to the CV results, the cathodic reductions of  $\text{Cu}_2\text{S}$  occurred in one step and NiS occurred in two steps:  $\text{Cu}_2\text{S} \Rightarrow \text{Cu}$  for copper reduction and  $\text{NiS} \Rightarrow \text{Ni}_3\text{S}_2 \Rightarrow \text{Ni}$  for nickel reduction.

2) Galvanostatic investigations showed that the applied currents did not significantly influence the obtained Cu–Ni alloy compositions, which had Cu/Ni mass ratios close to those of the charged sulfide mixtures.

3) Potentiostatic studies revealed that the sulfur content in the products depended on the applied voltage. It was possible to synthesize high-purity CuNi10 alloy containing a maximum sulfur content of  $60 \times 10^{-6}$  by electrolysis at 2.5 V for 15 min.

4) The desired compositions of the Cu–Ni alloys could be achieved by tuning the Cu/Ni mass ratios.

5) This developed DER technique could be applied for the recovery of heavy metals from precipitated sulfides produced in the mining and metallurgical industries during the treatment of process solutions, waste waters, and mining effluents.

## References

[1] DAVIS J R. Copper and copper alloys [M]. Ohio: ASM International, 2001.

[2] BUDINSKI K G, BUDINSKI M K. Copper and its alloys [C]// Engineering Materials: Properties and Selection. New Jersey: Prentice Hall, 2010.

[3] EVERHART J L. Copper-base nickel alloys [C]// Engineering properties of nickel and nickel alloys. New York: Plenum Press, 1971: 100–128.

[4] HABASHI F. Handbook of extractive metallurgy [M]. Weinheim: Wiley-VCH, 1997, 2: 491–580.

[5] MARK E S, MATTHEW J K, KATHRYN C. Extractive metallurgy of copper [M]. Amsterdam: Elsevier, 2011.

[6] VIGNES A. Metallurgical reaction processes [M]// Extractive Metallurgy 2. US: Wiley-ISTE, 2011: 255–291.

[7] HABASHI F. Pollution problems in the metallurgical industry: A review [J]. Journal of Mining & Environment, 2011, 2: 17–26.

[8] MOHANDAS K S. Direct electrochemical conversion of metal oxides to metal by molten salt electrolysis: A review [J]. Mineral Processing and Extractive Metallurgy, 2013, 122: 195–212.

[9] FRAY D J. Emerging molten salt technologies for metals production [J]. JOM, 2001, 53(10): 27–31.

[10] ABBASALIZADEH A, SEETHARAMAN S, TENG L, GRINDER O, IZUMI Y, BARATI M. Highlights of the salt extraction process [J]. JOM, 2013, 65: 1552–1558.

[11] YAN X Y, FRAY D J. Molten salt electrolysis for sustainable metals extraction and materials processing—A review [M]// KUI S, MENG J. Electrolysis: Theory, types and applications. Nova Science Publishers, Inc., 2010: 255–302.

[12] SADOWAY D R. New opportunities for metals extraction and waste treatment by electrochemical processing in molten salts [J]. Journal of Materials Research, 1995, 10: 487–492.

[13] VISHNU D S M, SANIL N, SHAKILA L, SUDHA R, MOHANDAS K S, NAGARAJAN K. Electrochemical reduction of  $\text{TiO}_2$  powders in molten calcium chloride [J]. Electrochimica Acta, 2015, 159: 124–130.

[14] GAO Hai-ping, JIN Xian-bo, ZOU Si-wei, LING Feng-zi, PENG Jun-jun, WANG Zhi-yong, CHEN G Z. Liquid diffusion of the instantaneously released oxygen ion in the electrolytic porous Fe from solid  $\text{Fe}_2\text{O}_3$  in molten  $\text{CaCl}_2$  [J]. Electrochimica Acta, 2013, 107: 261–268.

[15] VISHNU D S M, SANIL N, MOHANDAS K S. Electrochemical conversion of solid  $\text{Nb}_2\text{O}_5$  to Nb in sodium chloride melt as proof of oxygen ionisation mechanism of electrodeoxidation [J]. Journal of Alloys and Compounds, 2016, 677: 258–265.

[16] LIU Zheng-wei, ZHANG Hong-ling, PEI Li-li, SHI Yi-lang, CAI Zai-hua, XU Hong-bin, ZHANG Yi. Direct electrolytic preparation of chromium metal in  $\text{CaCl}_2\text{--NaCl}$  eutectic salt [J]. Transactions of Nonferrous Metals Society of China, 2018, 28: 376–384.

[17] LI Guo-ming, JIN Xian-bo, WANG Di-hua, CHEN G Z. Affordable electrolytic ferrotitanium alloys with marine engineering potentials [J]. Journal of Alloys and Compounds, 2009, 482: 320–327.

[18] DAI L, WANG S, WANG L, YU Y, SHAO G. Preparation of ZrMn<sub>2</sub> hydrogen storage alloy by electro-deoxidation in molten calcium chloride [J]. Transactions of Nonferrous Metals Society of China, 2014, 24: 2883–2889.

[19] DAI Lei, WANG Shuo, LI Yue-hua, WANG Ling, SHAO Guang-jie. Direct electrochemical preparation of  $\text{CeCo}_5$  alloy from mixed oxides [J]. Transactions of Nonferrous Metals Society of China, 2012, 22: 2007–2013.

[20] SUN Xiu-yun, LU Gui-min, FAN Shu-di. Electrochemical mechanism of electrolysis codeposition of Mg–Sr alloy in molten salt [J]. Transactions of Nonferrous Metals Society of China, 2014, 24: 1629–1634.

[21] ZHANG Mi-lin, CAO Peng, HAN Wei, YAN Yong-de, CHEN Li-jun. Preparation of Mg–Li–La alloys by electrolysis in molten salt [J]. Transactions of Nonferrous Metals Society of China, 2012, 22: 16–22.

[22] SUREA J, VISHNU D S M, SCHWAND C. Direct electrochemical synthesis of high-entropy alloys from metal oxides [J]. Applied Materials Today, 2017, 9: 111–121.

[23] VISHNU D S M, SURE J, MOHANDAS K S. Corrosion of high density graphite anodes during direct electrochemical de-oxidation of solid oxides in molten  $\text{CaCl}_2$  medium [J]. Carbon, 2015, 93: 782–792.

[24] CHEN G Z, FRAY D, FARTHING T W. Direct electrochemical reduction of titanium dioxide to titanium in molten calcium chloride

- [J]. Nature, 2000, 407: 361–364.
- [25] NIE Xin-miao, DONG Ling-yan, BAI Chen-guang, CHEN Deng-fu. Preparation of Ti by direct electrochemical reduction of solid  $\text{TiO}_2$  and its reaction mechanism [J]. Transactions of Nonferrous Metals Society of China, 2006, 16: 723–727.
- [26] MOHANDAS K S, FRAY D. FFC cambridge process and removal of oxygen from metal-oxygen systems by molten salt electrolysis: An overview [J]. Transactions of the Indian Institute of Metals, 2004, 57: 579–592.
- [27] CHEN G Z. Forming metal powders by electrolysis [C]//CHANG I, ZHAO Y. Advances in Powder Metallurgy. Cambridge: Woodhead Publishing, 2013: 19–21.
- [28] CHEN G Z, FRAY D J. Cathodic refining in molten salts: Removal of oxygen, sulfur and selenium from static and flowing molten copper [J]. Journal of Applied Electrochemistry, 2001, 31: 155–164.
- [29] GE Xin-lei, WANG Xi-dong, SEETHARAMAN S. Copper extraction from copper ore by electro-reduction in molten  $\text{CaCl}_2$ -NaCl [J]. Electrochimica Acta, 2009, 54: 4397–4402.
- [30] LI Guo-ming, WANG Di-hua, JIN Xian-bo, CHEN G Z. Electrolysis of solid  $\text{MoS}_2$  in molten  $\text{CaCl}_2$  for Mo extraction without  $\text{CO}_2$  emission [J]. Electrochemistry Communications, 2007, 9: 1951–1957.
- [31] GAO Hai-ping, TAN Ming-sheng, RONG Liang-bin, WANG Zhi-yong, PENG Jun-jun, JIN Xian-bo, CHEN G Z. Preparation of Mo nanopowders through electroreduction of solid  $\text{MoS}_2$  in molten  $\text{KCl}$ -NaCl [J]. Physical Chemistry Chemical Physics, 2014, 16: 19514–19521.
- [32] XIAO Y, van der PLAS D W, BOHTE J, LANS S C, VAN SANDWIJK A, REUTER M A. Electrowinning Al from  $\text{Al}_2\text{S}_3$  in molten salt [J]. Journal of The Electrochemical Society, 2007, 154: 334–338.
- [33] WANG Tao, GAO Hai-ping, JIN Xian-bo, CHEN Hua-lin, PENG Jun-jun, CHEN G Z. Electrolysis of solid metal sulfide to metal and sulfur in molten NaCl-KCl [J]. Electrochemistry Communications, 2011, 13: 1492–1495.
- [34] YIN H, CHUNG B, SADOWAY D R. Electrolysis of a molten semiconductor [J]. Nature Communications, 2016, 7: 12584–12589.
- [35] SUZUKI N, TANAKA M, NOGUCHI H, NATSUI S, KIKUCHI T, SUZUKI R O. Reduction of  $\text{TiS}_2$  by OS Process in  $\text{CaCl}_2$  Melt [J]. ECS Transactions, 2016, 75: 507–515.
- [36] MATSUZAKI T, SHUNGO N, SUZUKI R O. Electrolytic reduction of  $\text{V}_3\text{S}_4$  in molten  $\text{CaCl}_2$  [J]. Materials Transactions, 2017, 58(3): 371–376.
- [37] TAN Ming-sheng, HE Rui, YUAN Ya-ting, WANG Zhi-yong, JIN Xian-bo. Electrochemical sulfur removal from chalcopyrite in molten NaCl-KCl [J]. Electrochimica Acta, 2016, 213: 148–154.
- [38] SOKHANVARAN S, LEE S K, LAMBOTTE G, ALLANORE A. Electrochemistry of molten sulfides: Copper extraction from  $\text{BaS}$ - $\text{Cu}_2\text{S}$  [J]. Journal of The Electrochemical Society, 2016, 163: 115–120.
- [39] GE Xin-lei, SEETHARAMAN S. The salt extraction process—A novel route for metal extraction, Part 2—Cu/Fe extraction from copper oxide and sulphides [J]. Mineral Processing and Extractive Metallurgy, 2010, 119: 93–100.
- [40] GHARABAGHI M, IRANNAJAD M, AZADMEHR A R. Selective sulphide precipitation of heavy metals from acidic polymetallic aqueous solution by thioacetamide [J]. Industrial and Engineering Chemistry Research, 2012, 51: 954–963.

## $\text{CaCl}_2$ - $\text{Cu}_2\text{S}$ -NiS 熔盐电解生产 Cu-Ni 合金

Levent KARTAL<sup>1,2</sup>, Servet TIMUR<sup>1</sup>

1. Department of Metallurgical & Materials Engineering, Istanbul Technical University, 34469 Maslak, Istanbul, Turkey;

2. Department of Metallurgical & Materials Engineering, Hitit University, Corum, Turkey

**摘要:** 介绍一种金属/合金的生产方法, 用于恒电流和恒电位条件下由混合硫化物( $\text{Cu}_2\text{S}$ , NiS)生产 Cu-Ni 合金, 称为直接电化学还原(DER)。研究槽电压和槽电流等工艺参数对还原得到的化合物组成的影响, 以生产工业所需的 CuNi10, CuNi20 和 CuNi30 等合金。在 1200 °C 下采用循环伏安法(CV)考察  $\text{Cu}_2\text{S}$  和 NiS 在  $\text{CaCl}_2$  熔体中的电化行为。根据 CV 研究结果,  $\text{Cu}_2\text{S}$  的阴极还原是一步完成的, 即  $\text{Cu}_2\text{S} \Rightarrow \text{Cu}$ ; NiS 的阴极还原则分两步进行, 即  $\text{NiS} \Rightarrow \text{Ni}_3\text{S}_2 \Rightarrow \text{Ni}$ 。恒电流研究表明, 在 10 A 电流下电解 15 min, 可制备出最高硫含量为  $320 \times 10^{-6}$  的高纯 CuNi10 合金。扫描电子显微镜以及能量色散 X 射线能谱和光学发射光谱(OES)测试结果表明, 在 2.5 V 电压下直接电化学还原 15 min, 可制备出杂质含量低(即硫含量小于  $60 \times 10^{-6}$ )的所选成分的 Cu-Ni 合金。

**关键词:** 熔盐电解; 电还原; 铜提取; 硫化铜; 硫化镍; Cu-Ni 合金

(Edited by Xiang-qun LI)